RADC-TDR-63-110

January, 1963

FINAL TECHNICAL REPORT

C-BAND, WIDEBAND SOLID STATE AMPLIFIER

by

Harvey M. Endler

Micromega CORPORATION

VENICE, CALIFORNIA

Contract No. AF 30(602)-2525

Prepared

for

ROME AIR DEVELOPMENT CENTER

RESEARCH AND TECHNOLOGY DIVISION

AIR FORCE SYSTEMS COMMAND

UNITED STATES AIR FORCE

GRIFFISS AIR FORCE BASE

NEW YORK

Title of Report RADC-TDR-63-110

PUBLICATION REVIEW

This report has been reviewed and is approved.

Approved: Edward N. Munzer
EDWARD N. MUNZER
Chief, Electronic Warfare Laboratory
Directorate of Intelligence & Electronic Warfare

Approved: Robert J. Quinn
ROBERT J. QUINN, JR., Col, USAF
Director of Intelligence & Electronic Warfare

FOR THE COMMANDER: Irving J. Gabelman
IRVING J. GABELMAN
Director of Advanced Studies

RADC-TDR-63-110

January, 1963

FINAL TECHNICAL REPORT

C-BAND, WIDEBAND SOLID STATE AMPLIFIER

by

Harvey M. Endler

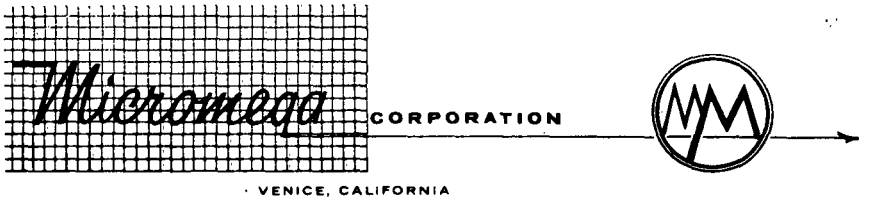

Contract No. AF 30(602)-2525

Project No. 5573

Task No. 557301

prepared

for

ROME AIR DEVELOPMENT CENTER
RESEARCH AND TECHNOLOGY DIVISION
AIR FORCE SYSTEMS COMMAND
UNITED STATES AIR FORCE

GRIFFISS AIR FORCE BASE
NEW YORK

FOREWORD

Acknowledgement is given to Mr. C. E. Nelson who derived the theory and is responsible for the design of the broadband amplifier.

ABSTRACT

This is the final report on a program to develop two experimental models of a low noise diode parametric amplifier. The first amplifier is fixed tuned with an instantaneous amplifying bandwidth from 4000 to 6000 mcps, and the second is to have an instantaneous bandwidth of 15 mcps, electronically tunable, from 4000 to 6000 mcps. Both units are to have noise figures under 3 db across the specified frequency range. In addition, both units are to have high operational stability, large dynamic range, freedom from spurious responses, and be applicable to either pulse or continuous wave (cw) signals.

It was shown in the first quarterly report that both amplifiers are theoretically limited by the bandwidth of the amplifier signal circuit, and 2000 mcps range was not to be expected from either unit. During the development phase, additional practical difficulties showed themselves, and it was not possible to achieve the theoretically predicted bandwidths. Best results obtained from the broadband unit are 900 mcps bandwidth, at 12 db gain, and about 600 mcps bandwidth at 17 db gain. The electronically tunable unit will tune about 900 mcps at 20 db gain, with additional qualifications that are discussed in the report. Noise figures are under 4 db at all frequencies, with a minimum noise figure of 2.5db achieved in both amplifiers at certain frequencies. The remainder of the electrical specifications have essentially been achieved, and are discussed in this report.

CONTENTS

LIST OF ILLUSTRATIONS

PUBLICATIONS

1. First Quarterly Technical Note, "C-Band Wideband Solid State Amplifier," RADC-TR-61-279, Micromega Corp., Sept. 15, 1961.

2. Second Quarterly Technical Note, RADC-TDR-62-110; December 15, 1961.

3. Third Quarterly Technical Note, RADC-TDR-62-318; March 15, 1962.

4. Fourth Quarterly Technical Note, RADC-TDR-62-593; June 15, 1962.

5. "Broadband Parametric Amplifier," Cover Story, MICROWAVES, October 1962, pg. 48.

A. INTRODUCTION

During the past few years, parametric amplifiers have been used mainly as retrofits for the previous generation of radar systems. With the advent of more sophisticated radars, principally those which are based on rapidly varying frequency shifting over wide microwave bandwidths, the need for more advanced types of parametric amplifiers has arisen.

Purpose of this contract was to develop two new designs in parametric amplifiers: The first is an extremely wide band low noise amplifier, and the second is a narrow band unit, rapidly electronically tunable over wide frequency ranges. Both units are to be one-port types, that is, with the amplified output signal at the same frequency as the input signal.

Design objective for both amplifiers was a frequency range of 2000 mcps, from 4000 to 6000 mcps, in the first case for instantaneous bandwidth, and in the second for electronic tuning range. Early theoretical calculations showed that the full 2000 mcps range was not to be expected from either unit, due primarily to limitations on the bandwidth of the amplifier signal circuit with currently available varactor diodes (Ref. 1). The final experimental results fall short of the theoretical expectations because of practical difficulties which became apparent as the design work progressed. This is discussed in the text, along with knowledge gained during the development phase which might eventually lead to a full 2000 mcps amplifier.

Both final amplifiers represent a compromise, since more bandwidth could have been obtained in either case if noise figure had been allowed to deteriorate. A maximum of 4 db was allowed for noise figure at any frequency in the range, and over 90% of their frequency ranges, both amplifiers exhibit noise figures under 3.5 db. Typical bandwidth for the wideband amplifier is 900 mcps at 12 db gain, or 600 mcps at 17 db gain. The tunable unit, with the present BWO pump source, tunes 900 mcps at 18 db gain. Bandwidths are to the 3 db points, and maximum ripple within the band is less than 3 db.

B. DISCUSSION

1. BROADBAND PARAMETRIC AMPLIFIER

A. DESCRIPTION

A photograph of the final configuration of the broadband amplifier is given in Figure 1. Component parts of the unit are made of brass, and the whole assembly is mounted to an aluminum base plate. Input to the amplifier is through RG/49U waveguide, and output is type N, but either type of transmission line is readily usable at either port through the use of waveguide to coaxial adapters. Incoming signal circulates clockwise through the input circulator, entering the amplifier signal circuit. Amplified signal passes out of the third port of the input circulator, through the biasing tee, and circulates counterclockwise through the output circulator which serves as an output isolator. The third port of the output circulator is terminated in a matched coaxial load to absorb reflections from the mixer or other detector which follows the parametric amplifier.

The pump klystron, with its associated blower, can be seen near the center of the photograph. Following the klystron in the pump line are a reverse-hole directional coupler with a built-in crystal detector (pump power monitoring system), a variable K-band attenuator (gain control), and a three-screw matching section to transform varactor impedance to the level of the waveguide impedance. The micrometer tuner on the opposite side of the amplifier block serves as a fine adjustment on pump match. Both the K-band pump monitor system and attenuator are specially designed, and are somewhat unique because of their size: the attenuator is 1.0 inches long, gives at least 25 db attenuation, and is well matched over a 400 mcps bandwidth at K-band. The directional coupler-crystal detector is flat over the same frequency range, with a coupling value of 15 db.

A 0-1 milliammeter in the aluminum housing provides pump power level indication. Also inside the aluminum housing is a three-volt dry cell which provides varactor bias. The remainder of the varactor DC bias circuitry consists of a 10-turn potentiometer, a polarity reversing

switch, and a 25-0-25 microammeter for monitoring the DC varactor current level. This circuitry is shown on the overall electrical schematic, Figure 2.

The biasing tee is a coaxial section with a shunt arm for injection of the DC varactor bias. A low pass filter in the shunt arm prevents leakage of RF power, and a series capacitance in the center conductor of the main arm prevents application of the bias voltage to the load on the output circulator. Biasing characteristics of the varactor are also independent of any DC impedance which may be attached to the amplifier output port. VSWR of the biasing tee is plotted as a function of frequency in Figure 3. VSWR of the input circulator looking in at the amplifier port is plotted in the same figure.

B. PERFORMANCE

Noise Figure

Figure 4 is a curve of measured amplifier noise figure as a function of frequency. This data has been corrected for

1) input circulator insertion loss, .15 db across the band

2) mixer - IF noise contribution.

The single-channel noise figure of the parametric amplifier alone is obtained by subtracting the mixer noise contribution from the overall receiver noise figure as computed from a standard Y-factor measurement:

$$F_{sc} = \frac{T_{ex}/T_o - 1}{Y - 1} - \frac{F_{M_{sc}} - 2}{G_s + G_{im}} \qquad (1)$$

(all symbols represent power ratios)

Y is measured Y-factor using a broadband argon noise lamp.

$\frac{T_{ex}}{T_o} - 1$ is the excess noise output of the argon noise lamp.

$F_{M_{sc}}$ = mixer single channel noise figure

= $^{2}F_{M_{dc}}$ (double channel)

G_s = amplifier power gain at the signal frequency = 17 db

G_{im} = amplifier gain at image frequency, including any image rejection: for an ideal image rejection mixer following the parametric amplifier, $G_{im} = 0$.

Noise figure was measured using first a broadband balanced mixer ($G_{im} \doteq G_s$), and secondly a broadband image-rejection balanced mixer. ($G_{im} \doteq 1$, since the image rejection was approximately equal to the parametric amplifier gain). Theory of operation and performance data for the image rejection mixer are described in Appendix I. The second-stage correction term is given by the second term on the right of equation (1). The broadband mixer-IF amplifier had a single channel noise figure of 10 db, and the correction term is:

$$\frac{F_{M_{sc}} - 2}{2G_s} = .08$$

The image rejection mixer-IF amplifier had a noise figure of 11 db, and the second stage noise contribution is:

$$\frac{F_{M_{sc}} - 2}{G_s + 1} = .157$$

Y-factors measured using the image-rejection mixer after the parametric amplifier were in general .15 db lower than those obtained with the broadband mixer. This is in good agreement with the respective correction factors as calculated above.

Note that the overall receiver noise figure is given by

$$F_{R_{sc}} = F_{PA_{sc}} \left(1 + \frac{G_{im}}{G_s} \right) + \frac{F_{M_{sc}} - 2}{G_s} \qquad (2)$$

For heterodyne receivers without image rejection, $G_{im} = G_s$, and equation (2) shows that the receiver noise figure will be 3 db higher than the parametric amplifier noise figure. For $G_{im} << G_s$ (image rejection), the receiver noise figure will be approximately equal to the parametric amplifier single channel noise figure.

Experimental values for amplifier noise figure may be used to estimate the varactor figure of merit. Varactor parameters will be required in the formulae for bandwidth in the next section. Using equation (97) of Reference 1,

$$F_{PA_{sc}} = 1 + \frac{G_o - 1}{G_o} \left\{ \frac{\frac{f_p}{f_i} - 1}{1 - \frac{f_s f_i}{\varphi^2}} \right\} \qquad (3)$$

where G_o = amplifier gain

f_p = pump frequency = 21.0 kmc

f_i = idler frequency = 15.5 kmc

f_s = center signal frequency = 5.5 kmc

$\varphi = e\, f_c = \frac{S_1}{S_o} \times f_c$ = normalized elastance nonlinearity x varactor cut-off frequency

Using F = 2.9 db (1.95), and solving equation (3)

$$\varphi = 16.7 \text{ gc}$$

For this value of φ, it is interesting to calculate the minimum theoretical noise figure if the "optimum" pumping frequency had been chosen. 21 kmc was chosen as a pump frequency in order to place the idler frequency at the self-resonant frequency of the available varactors. (This point will be discussed more fully in the next section.) From equation (99) of Reference (1), the optimum pumping frequency is

$$f_{p_{opt}} = \sqrt{f_s^2 + \varphi^2}$$

$$= 17.6 \text{ kmc}$$

and the theoretical minimum noise figure for this varactor, from reference (1), equation (98) is:

$$F_{min} = 1 + \frac{2 f_s}{f_{p_{opt}} - f_s}$$

$$= 1.908 = 2.8 \text{ db}$$

which is only .1 better than the measured value.

Values for φ and f_c, the diode cut-off frequency, will be needed for bandwidth calculations in the next section. The diode used for these measurements was an SD-22-7 (Semiconductor Devices, Inc.) and had a zero bias cut-off frequency of 70 kmc. Diode negative resistance is given by

$$R = \frac{\varphi^2}{f_c f_i (\omega_s C_o)} \tag{4}$$

and the diode loss resistance by

$$R_d = \frac{(\omega_i L_d) f_d^2}{f_i f_c} \tag{5}$$

where f_d is the diode self-resonant frequency and is approximately equal to the idler frequency.

Bandwidth

Equations are derived in the First Quarterly Report giving the normalized overall amplifier bandwidth as a function of gain. One set of equations assumes a zero reactance idler circuit, and the second assumes a zero reactance signal circuit. These equations represent the respective bandwidths of the multi-tuned amplifier signal and idler circuits, but no equation is given for amplifier bandwidth as a function of both signal and idler circuits of finite width. Reference (5) presents an analysis for finite width signal and idler circuits, but the overall bandwidths of the two circuits are assumed equal, and the general case is not derived.

An interesting result can be derived from the equations for single tuned signal and idler circuits, equations (31) and (57b) of the First Quarterly Report.

Normalized bandwidth for a single tuned signal circuit, and very broadband idler circuit

$$= \frac{X_{sl}}{R} \quad v_{sc} = \frac{2}{\left[G_o^{1/2} - 1\right]\sqrt{1 - \frac{2}{G_o}}} \qquad (6)$$

Normalized bandwidth for a single tuned idler circuit, and very broadband signal circuit

$$= \frac{X_{il}}{R_d} \quad v_{ic} = \frac{2}{\left[G_o^{1/2} + 1\right]\sqrt{1 - \frac{2}{G_o}}} \qquad (7)$$

where G_o = amplifier center frequency power gain

R = negative resistance developed by varactor

R_d = diode loss resistance

X_{sl}, X_{il} = reactance of tuned signal, idler, circuit

v_{sc}, v_{ic} = absolute bandwidth / center frequency of signal and idler circuits = $\frac{BW}{f_o}$

For $G_o >> 1$, equations (6) and (7) become

$$\frac{X_{s1}}{R} \quad \frac{BW_s}{f_{s_o}} = \frac{2}{\sqrt{G_o}} \tag{8}$$

$$\frac{X_{i1}}{R_d} \quad \frac{BW_i}{f_{i_o}} = \frac{2}{\sqrt{G_o}} \tag{9}$$

and $\frac{X_{s1}}{R}$, $\frac{X_{i1}}{R_d}$ are approximately equal to the signal and idler circuit Q's, respectively.

Combining equations (8) and (9):

$$\frac{\sqrt{G_o}}{\frac{1}{BW_s} + \frac{1}{BW_i}} = \frac{2 f_s}{Q_s \left[1 + \frac{f_s}{f_i} \frac{Q_i}{Q_s}\right]} \tag{10}$$

If we formally identify

$$\frac{1}{BW_T} = \frac{1}{BW_s} + \frac{1}{BW_i} \tag{11}$$

then $$\sqrt{G_o}\ BW_T = \frac{2 f_s}{Q_s \left[1 + f_s / f_i \ Q_i / Q_s\right]} \tag{12}$$

Equation (12) is identically equal to the standard gain-bandwidth equation for single-tuned parametric amplifier circuits in the high gain case. See, for example, Reference (6).

Although Equation (11) cannot be derived from the multi-tuned circuit equations, it is believed to be approximately true. In fact, for the parametric amplifier described in this report, with a quadruply tuned signal circuit and a singly tuned idler circuit, experimental agreement is quite good, as is shown by the succeeding calculations.

From Equations (42) and (57) of Reference 1, for the case where the idler frequency is chosen near the diode self-resonant frequency:

$$BW_s = f_{so}\left(\frac{\varphi^2}{f_c f_i}\right) \frac{.766}{\left(G_o^{1/8} - 1\right)\left(1 - \frac{2}{G_o}\right)^{1/8}} \qquad (13)$$

$$BW_i = f_{io}\left(\frac{f_i}{f_c}\right) \frac{2}{\left(G_o^{1/2} + 1\right)\left(1 - \frac{2}{G_o}\right)^{1/2}} \qquad (14)$$

Calculations of these equations at 17 db and at 12 db amplifier gain are given in the table below:

	Gain	
	12 db	17 db
BW_S	2.63 kmc	1.73 kmc
BW_i	1.47 kmc	.850 kmc
BW_T (Equation 11)	943 mc	570 mc
BW_T (Experimental)	900 mc	500 mc

Agreement between the experimental results and Equation (11)

$$BW_T = \frac{BW_s \, BW_i}{BW_s + BW_i}$$

is seen to be quite good. The limiting effect of the idler circuit bandwidth on the overall amplifier bandwidth is also quite obvious. Sketches of the amplifier response at these two gain levels are presented in Figure 8.

A procedure for multituning the idler circuit was given on Page 7 of the Third Quarterly Technical Note. Experimental circuits similar to the one illustrated in Figure 8 of that report were tried. As pointed out in that report, difficulty was encountered in coupling of the multituned idler circuit to the varactor. When coupling was achieved, the general effect was a deterioration of amplifier noise figure and a large increase in the required pumping power. Both of these effects are predicted by the theory (See Ref. 1 and Ref. 8), since the idler circuit must be resistively loaded to achieve an increase in bandwidth.

Since multituning was unsuccessful, it was necessary to insure that the reactance slope of the idler cavity was minimized by using the diode package resonant frequency as the idler frequency, and to make this frequency as high as possible. The lead inductance of the internal diode stud was slightly reduced by partially "burying" the diode in the signal circuit center conductor, as discussed on Page 4 of the Third Quarterly Technical Note. A drawing of the final diode configuration is given in Figure 5, along with the equivalent electrical circuit in Figure 6. The impedance of the coaxial stub section as seen from the varactor junction is j 133 ohms at the idler frequency (15.5 gc) and j 29 ohms at the center signal frequency (5.5 gc). These are calculated results and are slightly inaccurate because of the residual reactance of a choke section which is physically part of this coaxial stub. At the idler, 133 ohms is high enough so the diode is not excessively influenced. At the signal frequency, j 29 ohms will resonate a capacitance of 1 $\mu\mu$f which is the approximate net capacitance of the varactor junction, the varactor cartridge capacitance, and the varactor parasitic inductance.

An approximate calculation of the diode lead inductance in its mount is possible. From equation (6) of the Fourth Quarterly Technical Note, the diode reactance at the signal frequency is approximately:

$$j\,\frac{-\dfrac{1}{\omega_s C_o}}{1+\dfrac{C_s}{C_o}} = -j\,29 \text{ at resonance} \qquad (15)$$

And since the idler is resonant almost completely within the varactor

$$j\,\frac{1}{\omega_i C_s} = j\left(\omega_i L_d - \frac{1}{\omega_i C_o}\right) \tag{16}$$

Solving (15) and (16) for L_d

$$L_d = \frac{1}{\omega_i^2 C_o}\left(\frac{1}{\frac{1}{29\omega_s C_o} - 1} + 1\right) \tag{17}$$

taking $C_o = .25\ \mu\mu f$

then $L_d = .54$ nh

This value of $L_d = .2$ to $.3$ nh lower than is generally quoted for the standard diode package.

That the idler resonance is almost completely determined by the varactor is corroborated by the experimental behavior of the amplifier. With the diode self-biased through an external resistor, an increase in pumping power causes the amplifier gain to peak on the high frequency end of the band, and a decrease in pump power causes gain at the low frequency end to increase. This is explained in the former case by the average capacitance of the varactor increasing due to the forward self-bias developed, with a consequent lowering of the center idler resonant frequency and a resultant raising of the center signal frequency (for fixed pump frequency). Similarly, for decreasing pump power the center idler frequency is raised and the center signal frequency consequently lowered. The same effect is noted if a small forward or negative external bias voltage is applied to the varactor This effect is sketched in Figure 7.

II. ELECTRONICALLY TUNABLE PARAMETRIC AMPLIFIER

A. DESCRIPTION

A photograph of the final configuration of the electronically tunable parametric amplifier is given in Figure 9. A waveguide circulator (RG 49/U) is used, and the same housing incorporates an isolator which is only three-fourths of an inch thick. The isolator is used on the output side to prevent undesirable interactions which can occur if a badly mismatched mixer is attached to the parametric amplifier. Since the parametric amplifier signal circuit is in coaxial transmission line, a waveguide/coax adapter is required.

The wire seen emerging through the varactor bias plug on the amplifier signal circuit is a DC connection to the varactor. It is shown short-circuited to the amplifier brass body, which is the normal mode of bias for this unit. The pump and idler waveguide (RG 53/U, .050" height) are perpendicular to the coaxial line, and the varactor diode is mounted at the junction of these two transmission lines. Soldered to the micrometer barrel is a choked circular plunger which serves as the idler tuner. Detailed drawings of the interior parts of these components are given in previous Technical Notes. (see references).

At the rear of the photograph is the backward wave oscillator pump source. This is followed by an E-plane waveguide bend and a small K-band attenuator which serves as the amplifier gain control. A blower is mounted under the anode structure on the backward wave oscillator. The entire unit is mounted on an aluminum base plate.

B. PERFORMANCE

A schematic electrical diagram is given in Figure 10. Three sets of adjustments are shown, signal circuit matching screws, a movable idler short, and a three-screw pump matching tuner. If the power output spectrum of the backward-wave-oscillator (BWO) were perfectly flat over the range of interest, 21 to 23 gc, these adjustments would be almost independent, but this is not the case. For uniform BWO power output, the adjustments would consist of

1. Selecting the idler frequency (fixed) to cause the idler short to be 3/4 of a guide wavelength behind the varactor at the center pump frequency. This condition prevents the idler short from interfering with the pumping of the varactor.

2. Adjusting the pump matching screws for maximally flat pump power transmission to the varactor over as wide a frequency band as possible.

3. Adjusting the signal circuit tuning screws for maximally flat (or Tschebyscheff) response over the widest frequency band consistent with good noise figure.

Figure 11 is a typical curve of BWO frequency and power output as a function of helix voltage for a particular anode voltage. A definite power slope is indicated, but there is also a fine grain variation superimposed upon this. The rapid power fluctuations are due partially to the BWO itself, and partially to VSWR's in components between the tube and the amplifier proper. At 20 db nominal gain, the amplifier gain sensitivity is approximately ±1 db for ±.1 db pump power variation, as determined from the equation

$$G = \frac{\left(1 + \frac{P}{P_{CRIT}}\right)^2}{\left(1 - \frac{P}{P_{CRIT}}\right)^2} \qquad (18)$$

where P_{CRIT} is the pump power level which causes oscillation. It is easily seen that either or both of the first two adjustments above can be used to compensate for the slope in the BWO power characteristic. The signal circuit adjustment is also available, since required pump power is a function of signal circuit impedance levels.

Experimentally, it was found that widest band performance could be obtained by a careful adjustment of all three variables listed above. Gain can be kept at 18 db ± 2 db over the range 5300 - 5800 mc as the BWO sweeps from 21.9 to 22.4 gc. An additional 100 mc can be gained at each end of this range if a slight pump power readjustment is allowed, but beyond this range a mechanical signal circuit readjustment is required to maintain the noise figure. A typical plot of noise figure and instantaneous bandwidth is given in Figure 12.

C. CONCLUSIONS

The bandwidth and tuning range performance of the present two parametric amplifiers exceeds reported results obtained with any other varactor diode-type parametric amplifier at C-band. This includes other schemes which have been tried, such as travelling wave types, up-converters, multi-varactor types, and varactor-bias-tunable amplifiers. Although the full 2000 mcps bandwidths which were the objective of this development have not been achieved, it is felt that a significant contribution has been made, and that some insight has been obtained which will eventually lead to much broader bandwidth parametric amplifiers.

Each of the parametric amplifiers reported here still has one problem which might cause some hesitancy in wide scope systems usage of the device. For the broadband amplifier, this problem is the varactor diode. Careful selection has gone into each varactor for the experimental amplifier, and exact specifications for varactor parameters are still somewhat nebulous. The difficulty is believed to lie in the variation of C_1/C_o from varactor to varactor. Diode selection for the electronically tunable parametric amplifier is considerably less critical, since this amplifier does not depend upon a self-resonant idler circuit. The difficulty in the electronically tunable unit lies in the high degree of stabilization required for the BWO voltages, generally available only in laboratory power supplies.

D. RECOMMENDATIONS

Principle direction of further effort on the broadband amplifier should lie in increasing the bandwidth of the idler circuit, whereas the electronically tunable amplifier is limited by the bandwidths of both the signal and pump circuits. Attempts at multi-tuning the idler circuit of the broadband amplifier in general led to greatly deteriorated noise figures, and made the varactor much harder to pump. Both of these effects are predicted by the theory, since as shown in Reference 1, the idler circuit must be resistively loaded in order to achieve multi-tuning. Further bandwidth improvements, without noise figure deterioration, can be obtained with higher cut-off frequency varactor diodes, as they become available. Experimental work in improving the varactor mount is also indicated, since the parasitic inductance of the varactor can be reduced by manipulation of its external physical environment.

The electronically tunable parametric amplifier can be improved upon by adding a programming voltage to the grid of the backward wave oscillator pump source to control its power output as it sweeps in frequency. By this means, the parametric amplifier gain can be made uniform over much wider frequency tuning ranges. This scheme, in effect, also compensates for limitations of the bandwidth and flatness of the pump matching circuit into the varactor. Signal circuit bandwidth of this amplifier can be increased by utilizing the methods employed in the broadband parametric amplifier. In the broadband amplifier, quarter-wave spaced parallel resonators were utilized because of their relative ease of practical realization. It is expected that even greater signal circuit bandwidths can be obtained with direct-coupled cavity techniques.

APPENDIX I

IMAGELESS MIXERS

As shown in equation (2) on page 5 , the system noise figure of a heterodyne receiver employing broadband preamplification can be degraded as much as 3 db if image frequency noise is not attenuated. The mixer used for the measurements was a broadband balanced phase cancellation type. Operation of an unbalanced phase-cancellation mixer will be described here, but the balanced mixer is only slightly more complex.

A schematic diagram of the mixer is given in Figure (13). See Reference 7 . Voltages at various points labeled in the figure are listed below, where subscripts s, i, and LO pertain to signal, image and local oscillator frequencies, and k is the conversion efficiencies of the mixers.

at A

$$E_s \cos (\omega_s t - 90^\circ) + E_i \cos (\omega_i t - 90^\circ) \qquad \text{(I-1)}$$

at B

$$E_s \cos \omega_s t + E_i \cos \omega_i t \qquad \text{(I-2)}$$

For no differential LO phase shift between the mixers

at C

$$k E_s \cos (\omega_{LO} t - \omega_s t + 90^\circ) + k E_i \cos (\omega_{LO} t - \omega_i t + 90^\circ) \qquad \text{(I-3)}$$

at D

$$k E_s \cos (\omega_{LO} t - \omega_s t) + k E_i \cos (\omega_{LO} t - \omega_i t) = k E_s \cos \omega_{IF} t + k E_i \cos \omega_{IF} t \qquad \text{(I-4)}$$

at E

$$k\ E_s \cos(\omega_{IF}t - 90^\circ) + kE_i \cos(\omega_{IF}t - 90^\circ)$$

$$= k\ E_s \sin \omega_{IF}t + k\ E_i \sin \omega_{IF}t \qquad \text{(I-5)}$$

Phase of the output at C will depend on whether

$$(1)\quad \omega_i > \omega_{LO} > \omega_s \qquad \text{(I-6)}$$

or

$$(2)\quad \omega_s > \omega_{LO} > \omega_i \qquad \text{(I-7)}$$

For the first case, the output at C is

$$-k\ E_s \sin \omega_{IF}t + k\ E_i \sin \omega_{IF}t \qquad \text{(I-8)}$$

For the second case, output at C is

$$k\ E_s \sin \omega_{IF}t - k\ E_i \sin \omega_{IF}t \qquad \text{(I-9)}$$

For case (1), equations I-5 and I-8 show that signal addition and image cancellation are obtained if the output is taken from the difference port of the hybrid. For case (2), equations I-5 and I-9, signal addition and image cancellation are obtained when the output is taken from the sum arm of the hybrid. For convenience, the hybrid outputs may be made switchable to accommodate a local oscillator frequency either above or below the signal frequency.

Experimentally, the unit gave at least 15 db image rejection between 5 and 6 kmcps. For large signal drive levels, a saturation occurred in the mixer crystals which resulted in a reversal of the signal and image channels through the mixer.

REFERENCES

1. C. E Nelson, "C-Band, Wideband Solid State Amplifier," First Quarterly Technical Note, RADC-TR-61-279, Micromega Corp.; Sept. 15, 1961.

2. " Second Quarterly Technical Note, RADC-TDR-62-110; December 15, 1961.

3. " Third Quarterly Technical Note, RADC-TDR-62-318; March 15, 1962.

4. " Fourth Quarterly Technical Note, RADC-TDR-62-593; June 15, 1962.

5. A. Mayer, "Design of Single Diode Wideband Parametric Amplifiers of Specified Gain, Bandwidth, and Signal Load Impedance," Sylvania Electronic Defense Laboratories Technical Memorandum EDL-M353; Sept. 15, 1961.

6. P. P. Lombardo, E. W Sard, "Low Noise Microwave Reactance Amplifiers With Large Gain-Bandwidth Products," 1959 I.R.E. WESCON Convention Record (pt. 1); page 83.

7. R. B Wilds, "Microwave Two-Phase Converters For Imageless Receivers," Microwave Journal, September, 1961. Pg. 84.

8. P. Penfield, Jr., "Fundamental Limits of Varactor Parametric Amplifiers," Microwave Associates Report; August 15, 1960.

A more complete bibliography is included in Reference 1.

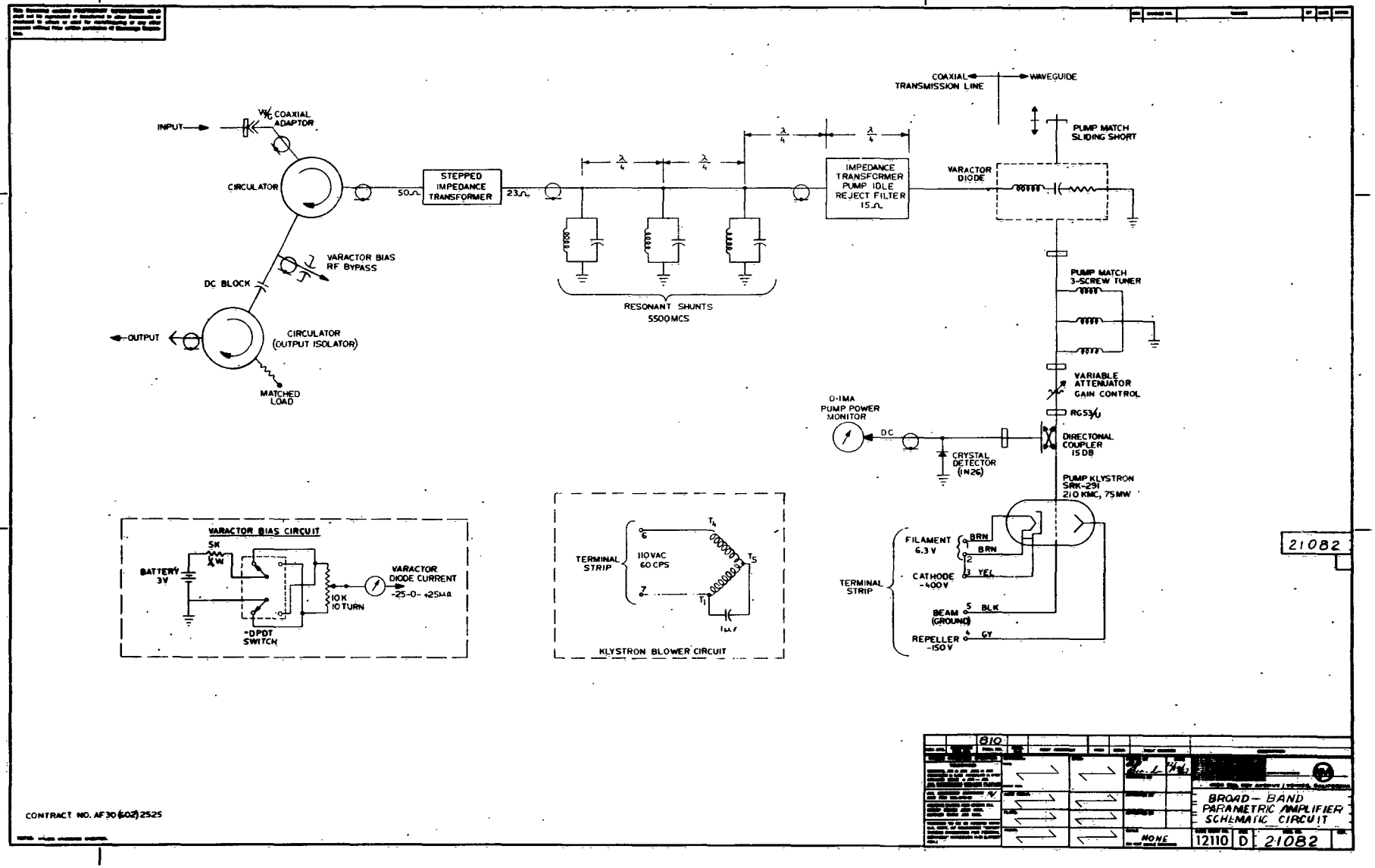

Figure 2. Schematic Diagram of Broadband Parametric Amplifier

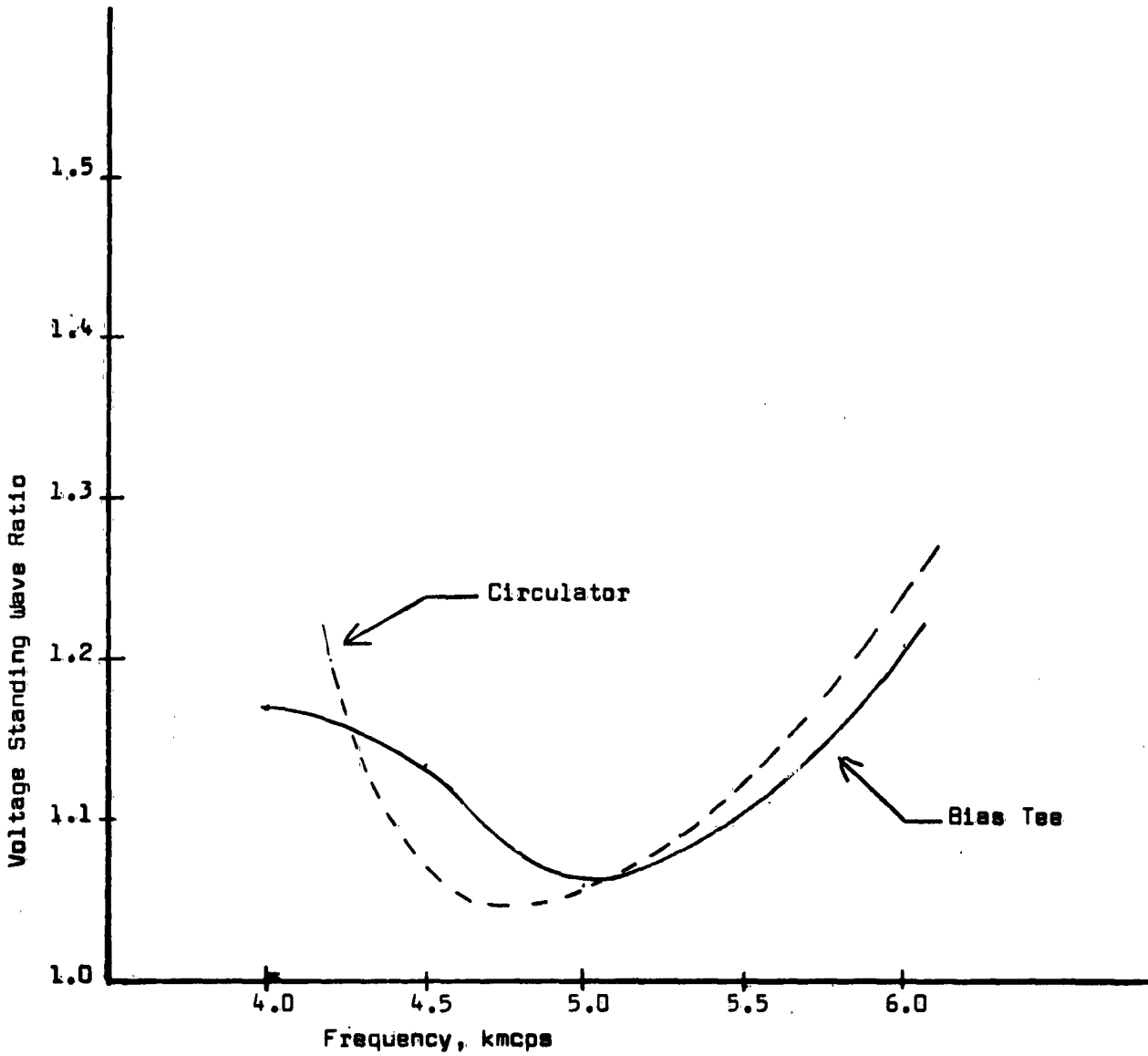

FIGURE 3. VSWR of Biasing Tee and Input Circulator (Amplifier Port) Broadband Parametric Amplifier

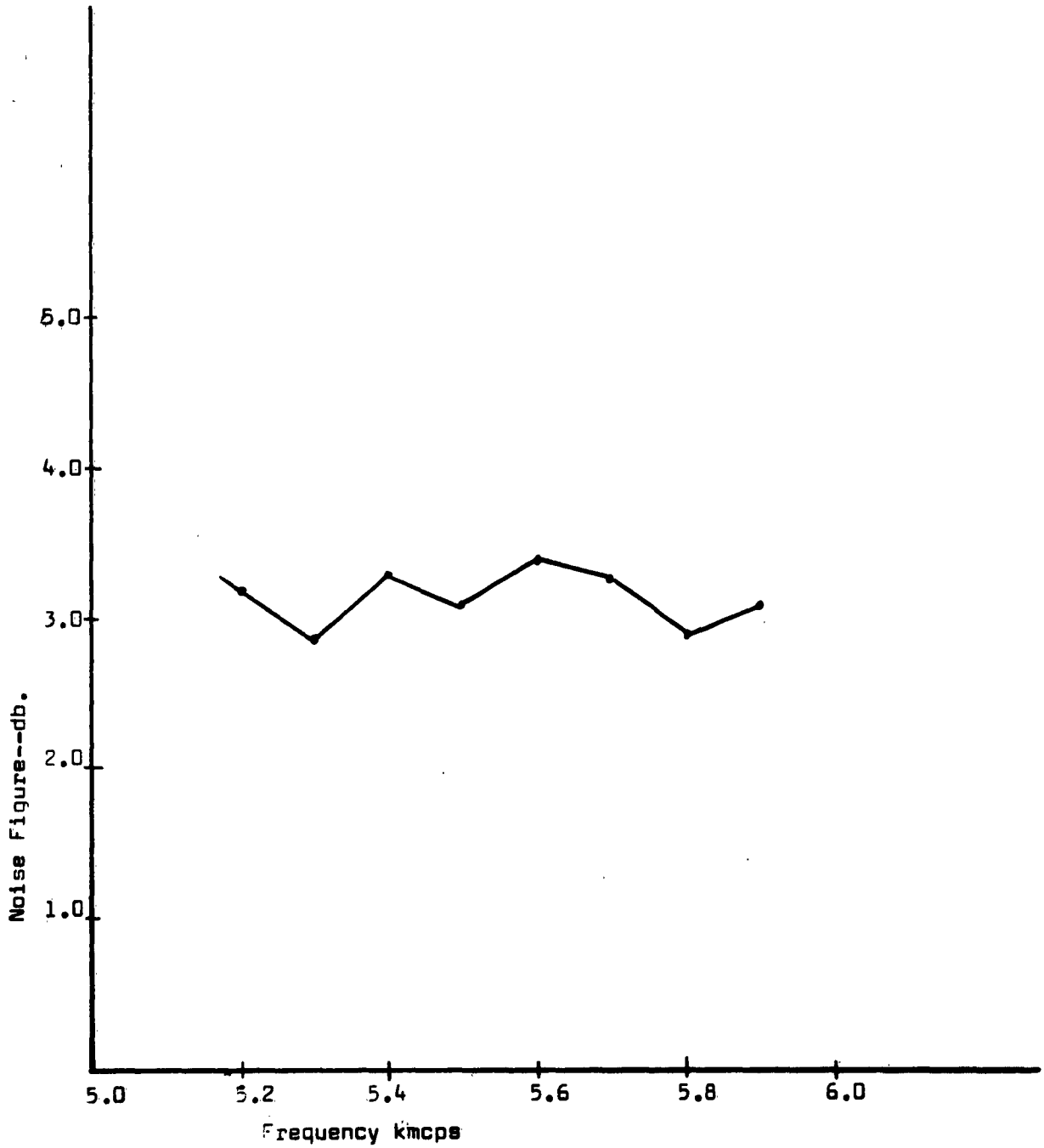

Figure 4. Broadband Parametric Amplifier Single Channel Noise Figure

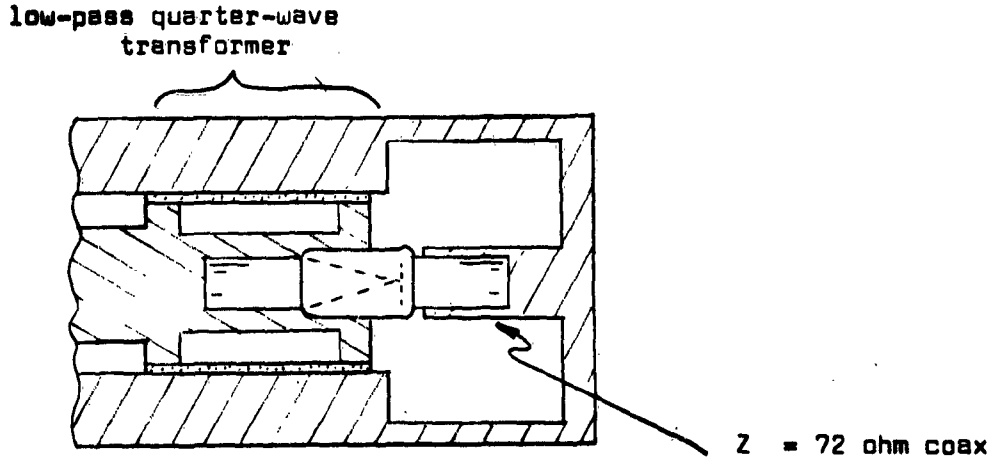

FIGURE 5

Microwave Diode Resonant Circuit

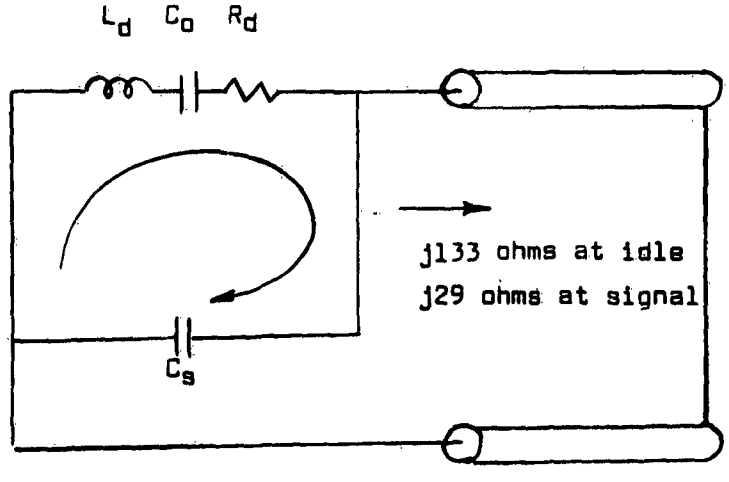

FIGURE 6

Equivalent Diode Mount Circuit

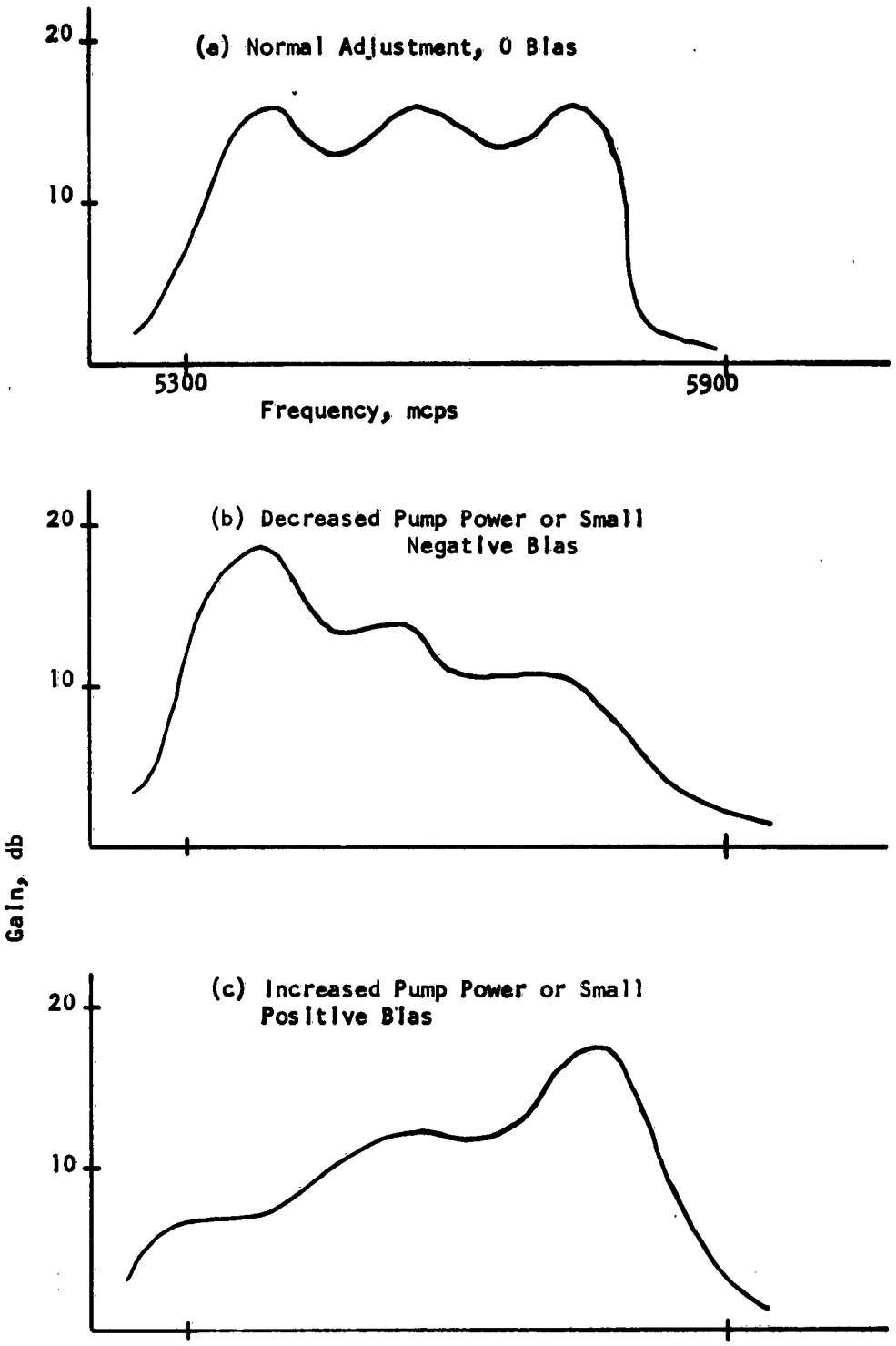

Figure 7. Broadband Amplifier Tuning Characteristics

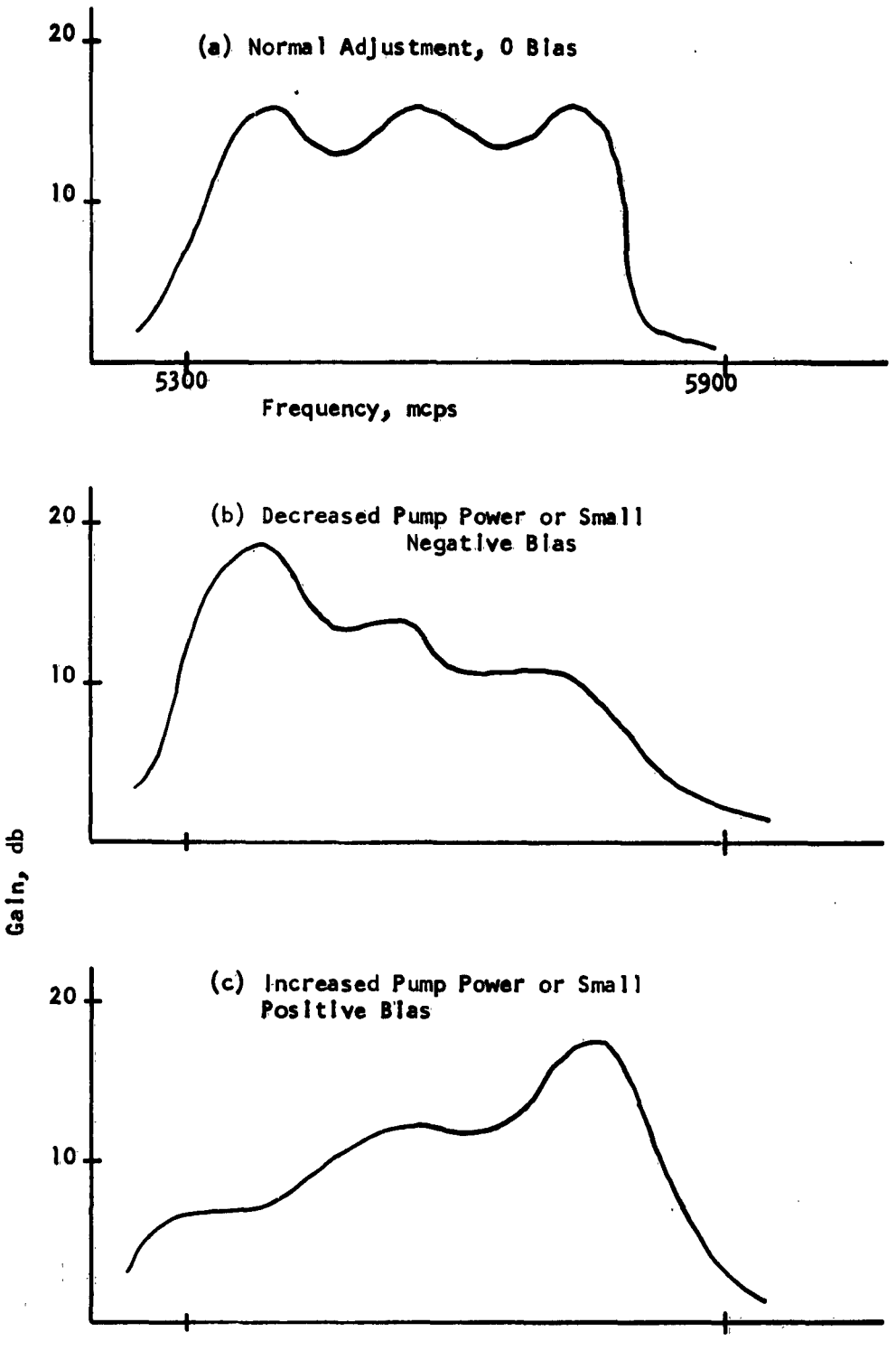

Figure 7. Broadband Amplifier Tuning Characteristics

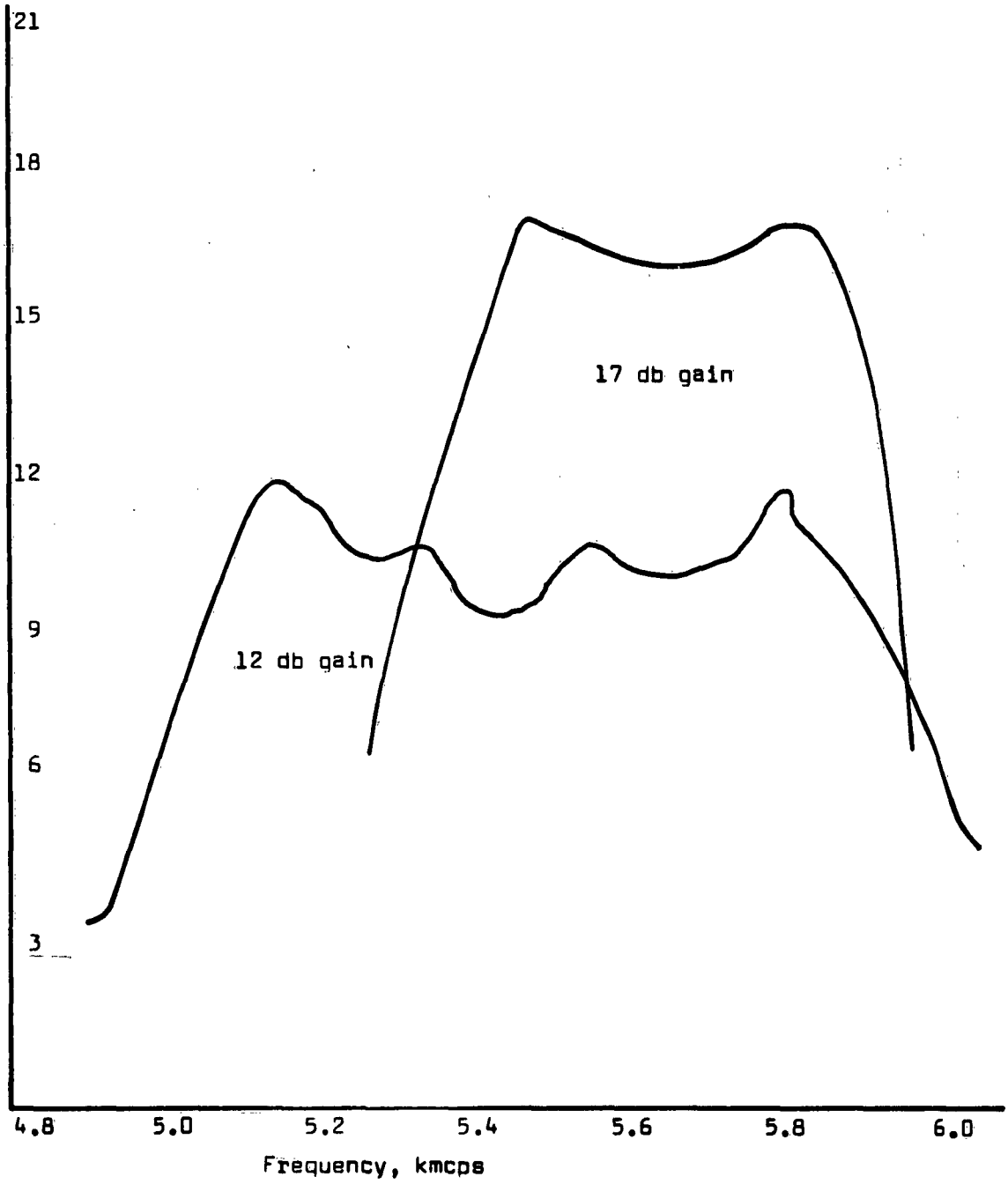

FIGURE 8

PARAMETRIC AMPLIFIER GAIN RESPONSE

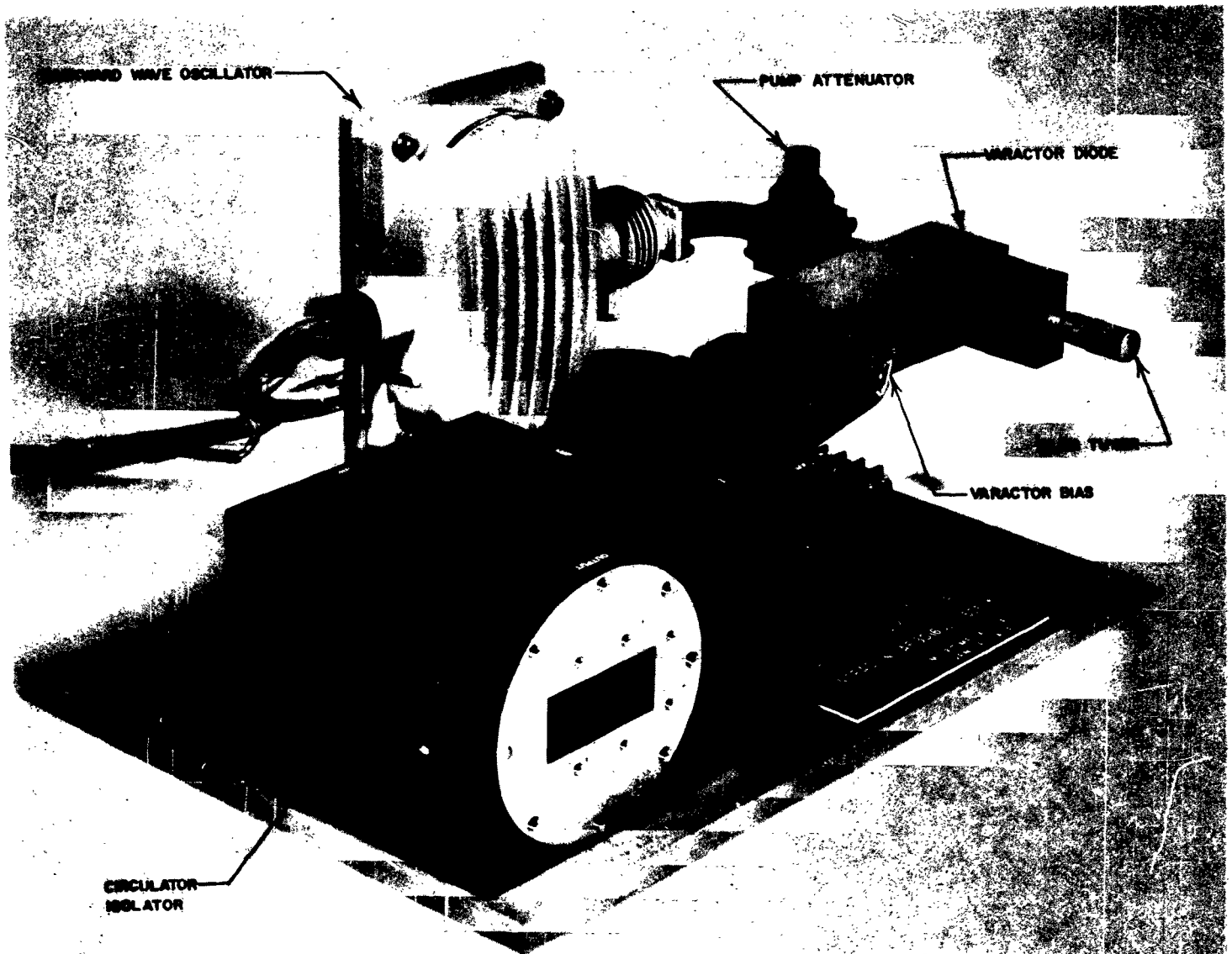

Figure 9. Photograph of Electronically Tunable Parametric Amplifier

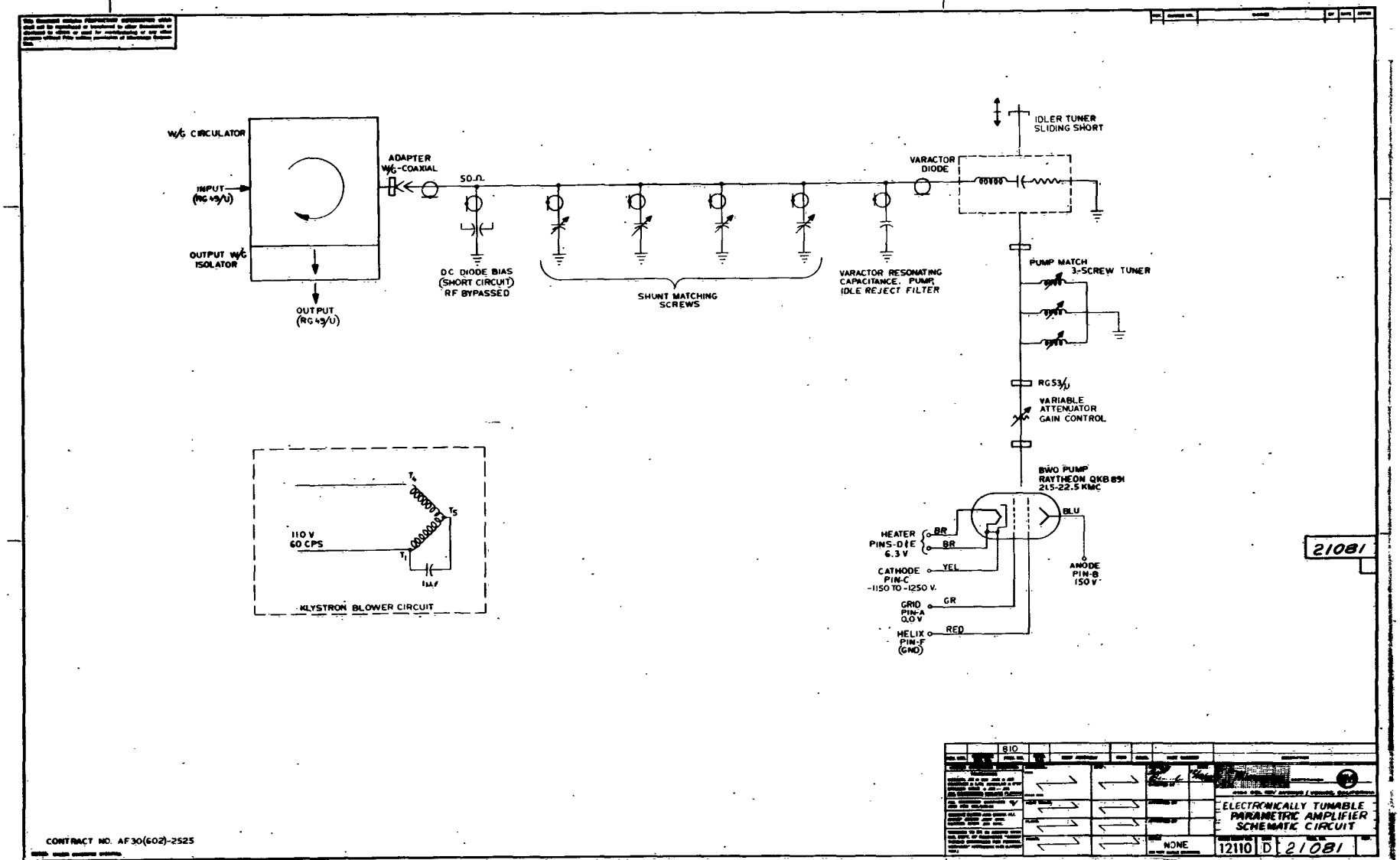

Figure 10. Schematic Diagram of Electronically Tunable Parametric Amplifier

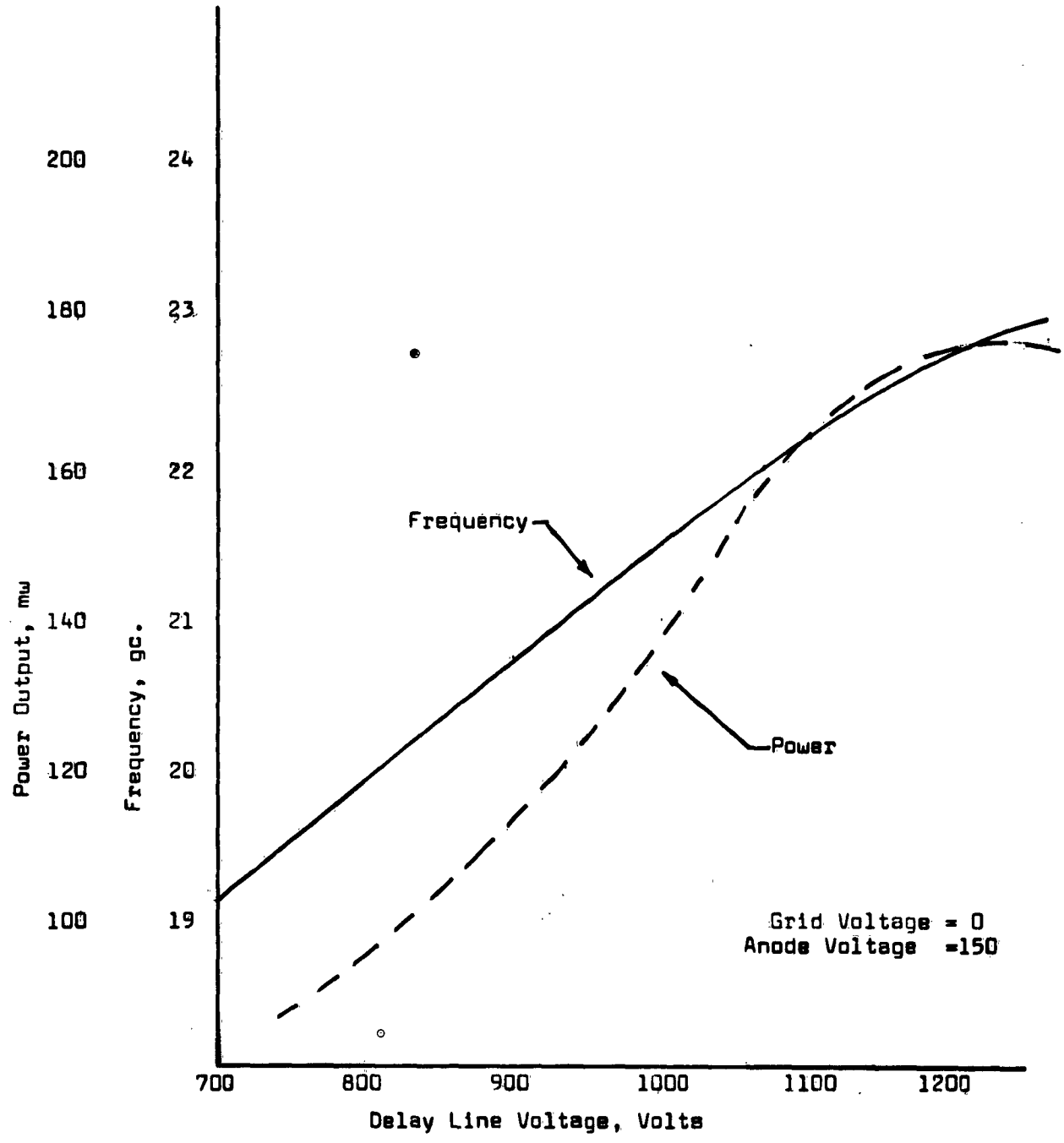

Figure 11. Backward Wave Oscillator (QK8 891) Chacteristics

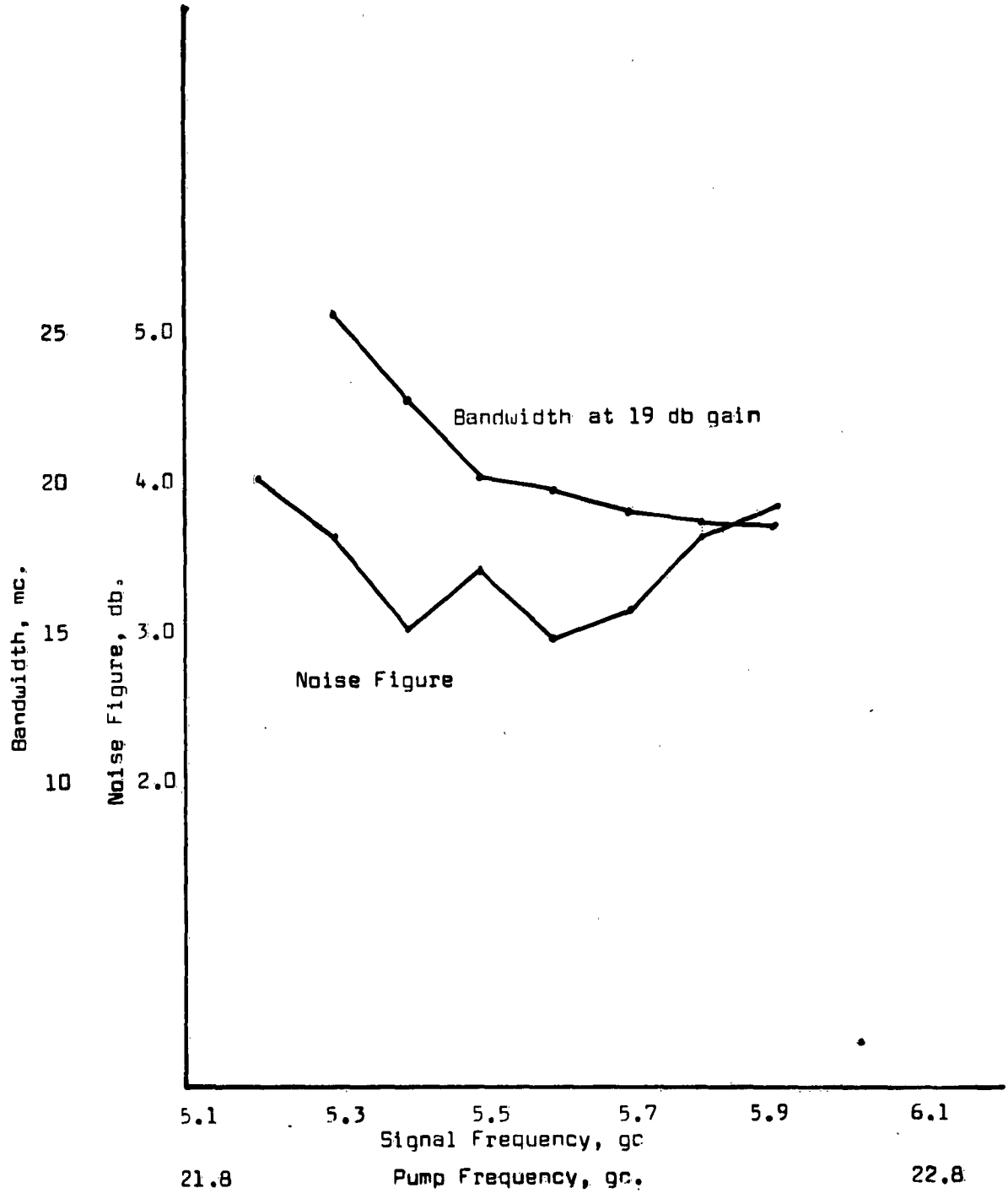

FIGURE 12. Noise Figure and Bandwidth of Electronically Tunable Parametric Amplifier

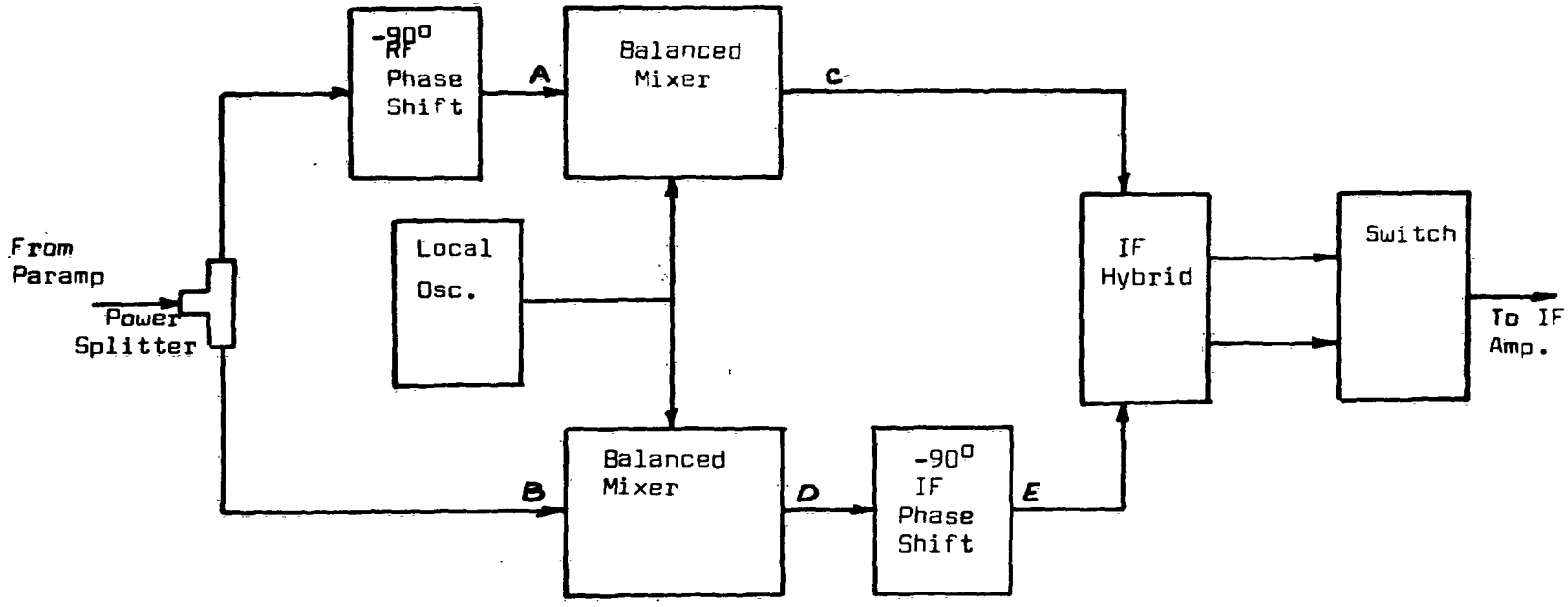

FIGURE 13. Schematic of Image-Rejection Mixer

DISTRIBUTION LIST FOR RADC TDR-63-110

	Nr. of Copies
RADC(RAWED ATTN: H. Friedman) Griffiss AFB NY	2
RADC (RAAPT) Griffiss AFB NY	1
RADC (RAALD) Griffiss AFB NY	1
GEEIA (ROZMCAT) Griffiss AFB NY	1
RADC (RAIS, ATTN: Mr. Malloy) Griffiss AFB NY	1
US Army Electronics R&D Labs Liaison Officer RADC Griffiss AFB NY	1
AUL (3T) Maxwell AFB Ala	1
ASD (ASAPRD) Wright-Patterson AFB Ohio	1
Chief, Naval Research Lab ATTN: Code 2027 Wash 25 DC	1
Air Force Field Representative Naval Research Lab ATTN: Code 1010 Wash 25 DC	1

	Nr. of Copies
Commanding Officer US Army Electronics R&D Labs ATTN: SELRA/SL-ADT Ft Monmouth NJ	1
National Aeronautics & Space Admin Langley Research Center Langley Station Hampton Virginia ATTN: Librarian	1
AFSC (SCSE) Andrews AFB Wash 25 DC	1
Commanding General US Army Electronics Proving Ground ATTN: Technical Documents Library Ft Huachuca Ariz	1
ASTIA (TISIA-2) Arlington Hall Station Arlington 12 VA	10
AFSC (SCFRE) Andrews AFB Wash 25 DC	1
Hq USAF (AFCOA) Wash 25 DC	1
AFOSR (SRAS/Dr. G.R. Eber) Holloman AFB NMex	1

	Nr. of Copies
Commanding General White Sands Missile Range NMexico ATTN: Technical Library	1
Director US Army Engineer R&D Labs Technical Documents Center Ft Belvoir Va	1
ESD (ESRL) L G Hanscom Fld Bedford Mass	1
Commanding Officer & Director US Navy Electronics Lab (LIB) San Diego 52 Calif	1
ESD (ESAT) LG Hanscom Fld Bedford Mass	1
AFSWC (SWOI) Kirtland AFB NMex	1
General Electric Co Attn: Mr. F. C. Dyer, Jr. 316 E. 9th St Owensboro, Ken	1
SFD Labs Inc 800 Rahway Ave Union NJ	1

	Nr. of Copies
Office of Chief of Naval Operations (Op-724) Navy Dept Wash 25 DC	1
Commander US Naval Air Dev Cen (NADC Lib) Johnsville Pa	1
Commander Naval Missile Center Tech Library (Code No. 3022) Pt. Mugu Calif	1
Bureau of Naval Weapons Main Navy Bldg Wash 25 DC ATTN: Technical Librarian, DL1-3	1
Redstone Scientific Information Center US Army Missile Command Redstone Arsenal, Alabama	1
Commandant Armed Forces Staff College (Library) Norfolk 11 Va	1
ADC (ADOAC-DL) Ent AFB Colo	1
AFFTC (FTOOT) Edwards AFB Calif	1
Commander US Naval Ordnance Lab (Tech Lib) White Oak, Silver Springs Md	1

	Nr. of Copies
Melabs ATTN: Dr. P.H. Vartanian 3300 Hillview Ave Palo Alto Calif	1
Director National Security Agency ATTN: Code K33 Ft George Meade, Md	1
USAFSS San Antonio Tex	1
RTD (RTGS) Bolling AFB Wash 25 DC	1